JOURNAL OF GEOPHYSICAL RESEARCH, VOL. 103, NO. D4, PAGES 3801–3814, FEBRUARY 27, 1998

Adjoint sensitivity of the Earth's radiation budget in the NCEP medium-range forecasting model

Zhijin Li

Supercomputer Computations Research Institute, Florida State University, Tallahassee

I. M. Navon[1]

Department of Mathematics, Florida State University, Tallahassee

Abstract. We introduced an adjoint technique to study sensitivity of the Earth's radiation budget (ERB) to cloud cover, water vapor, atmospheric temperature, and the Earth's surface temperature. This technique allowed us to calculate the partial derivatives of a defined ERB function with respect to all of the above variables on the model grid points by a single calculation of the adjoint model. We employed the radiation model of the National Centers for Environmental Prediction medium-range forecasting system to perform such an adjoint sensitivity analysis. For clear sky the absorbed shortwave radiation (ASR) was much more sensitive to the water vapor in the middle troposphere at high latitudes in the summertime hemisphere than at the tropical and subtropical areas. The outgoing longwave radiation (OLR) was 1 order of magnitude more sensitive to water vapor mixing ratios in the upper troposphere than to those in the middle and lower troposphere. In the tropics, more than 80% of a perturbation increase in the Earth's surface emission was trapped by the clear-sky column atmosphere, while only about 60–70% is trapped at middle and high latitudes. Rapidly decreasing latitude bands of trapping were found within the subtropics, and the semipermanent troughs over the central oceans displayed a significant effect. For the case of cloudy sky the ASR was more sensitive to low clouds than to middle and high clouds. The most sensitive low clouds tended to be located at midlatitudes rather than in the tropical regions. The OLR, as expected, was most sensitive to high clouds and displayed similar sensitivity to middle clouds. The net ERB was most sensitive to low clouds at midlatitudes in the summer hemisphere. The relationship between the results obtained and the greenhouse effect over tropical oceans as well as the influence of clouds on the climate change were explored, and some model deficiencies were discussed.

1. Introduction

Observational studies have greatly improved our knowledge of the Earth's radiation budget (ERB). The Earth Radiation Budget Experiment (ERBE) [*Barkstrom*, 1984; *Barkstrom and Smith*, 1986] attempted to measure the energy balance of the Earth from space, with emphasis on understanding the role of clouds in the climate system. The concept of cloud radiative forcing (CRF) [*Cess and Potter*, 1987] was thus established, and many studies contributed to the quantitative description of cloud impacts on the climate and climate change [e.g., *Ramanathan et al.*, 1989; *Harrison et al.*, 1990; *Hartmann and Doelling*, 1991]. The clear-sky atmospheric greenhouse effect was also understood in a more quantitative way, and the dependence on the water vapor variability associated with the deep convection over the tropical oceans (the super greenhouse effect) was estimated [e.g., *Raval and Ramanathan*, 1989; *Stephens and Greenwald*, 1991; *Inamdar and Ramanathan*, 1994].

How do the processes of the atmosphere and Earth's surface control the ERB and its regional and time variations? Some studies have focused on answering this question [e.g., *Inamdar and Ramanathan*, 1994; *Kiehl*, 1994]. It is fair to say that we still possess only a partial understanding of this problem and that systematic and specific studies have become a pressing requirement. In the present study we will concentrate on how regional change of atmospheric constituents, such as water vapor and clouds, affects the ERB. The importance of spatial distributions of atmospheric constituents for radiation variations has been recognized in numerical and observational studies. *Kiehl and Briegleb* [1992] showed that the longwave (LW) radiation (terrestrial radiation) clear-sky fluxes are sensitive to upper tropospheric moisture. *Zhang et al.* [1995] argued that for the net LW fluxes the relative importance of clouds and water vapor significantly changes with latitude. An in-depth understanding of such effects is necessary for the analysis of climate change. For example, climate warming may cause a decrease in cloud fraction [*Cess et al.*, 1990], and the regional variation of sensitivity may lead to a regional dependence of the ERB response.

The atmospheric state is characterized by strong meridional and vertical variations. Associated with the land-sea contrast, there are also significant zonal variations, and the permanent and semipermanent troughs (low atmospheric pressure re-

[1]Also at Supercomputer Computations Research Institute, Florida State University, Tallahassee.

Paper number 97JD03631.
0148-0227/98/97JD-03631$09.00

gions) and ridges (high atmospheric pressure regions) dominate the zonal variations [*Palmén and Newton*, 1967]. The radiative properties of the Earth's surface such as the albedo also display strong regional variations. Such spatial heterogeneity exerts complex impacts on the radiation response. The understanding of such combined impacts is crucial for depicting ERB regional features.

One approach in examining the role of the atmospheric and Earth's surface processes is sensitivity analysis. Let R denote a function of the ERB, and let x denote the state variables of the atmospheric and Earth's surface such as cloud cover, water vapor mixed ratios, etc. We define the ratio $\Delta R/\Delta x$ as the sensitivity of R to x, where ΔR is the radiation response to the perturbation Δx. We can simply obtain sensitivities by directly running a radiation model; this approach is called direct sensitivity analysis. For example, *Slingo* [1990] and *Sinha and Shine* [1995] carried out such a direct sensitivity analysis of the ERB to clouds. However, when we require sensitivities to various model variables on every model grid point in order to investigate detailed spatial variations of sensitivity and to evaluate the relative sensitivity among various variables, direct sensitivity analysis becomes computationally prohibitive. One solution is to take advantage of the adjoint technique. Using this technique, we can calculate the partial derivatives of R with respect to x, i.e., $\lim_{\Delta x \to 0} \Delta R/\Delta x$, by a single calculation of the adjoint model which is derived from the original radiation model. Components of x can be all model variables on every model grid point [see *Cacuci*, 1981, 1987; *Zou et al.*, 1993]. We shall use this method to carry out sensitivity analysis of the ERB to cloud cover, water vapor, and atmospheric and Earth's surface (AES) temperatures.

The outline of this paper is as follows. Section 2 briefly describes the radiation model in the National Centers for Environmental Prediction (NCEP) medium-range weather forecasting system. In section 3 we formulate an adjoint sensitivity analysis method applicable to radiation models and then detail the derivation of the adjoint and linearized models, as well as the test of the correctness of the adjoint model and assessment of validity of linearization. Section 4 presents the results of adjoint sensitivity analysis. Finally, section 5 summarizes the results of this study. The general mathematical description of the adjoint sensitivity method is provided in Appendix A.

2. Radiation Model

The radiation codes employed in the following calculations are operationally used in the NCEP medium-range weather forecasting system [*Kanamitsu*, 1991]. The effects of the major radiatively active atmospheric constituents, including water vapor (H_2O), carbon dioxide (CO_2), ozone (O_3), and clouds, are taken into account in the modeling of both shortwave (SW) and longwave (LW) processes. The output products of this model include layer radiative heating rates and upward SW and LW fluxes at top of the atmosphere, as well as downward LW and net SW fluxes at the Earth's surface. This model has $K = 28$ vertical layers and $J = 128 \times 62$ Gaussian grid points, i.e., a horizontal resolution of about 2.8125°.

The cloud parameterization is a diagnostic scheme based on the work of *Slingo* [1987]. The main difference between this parameterization and Slingo's scheme and its performance are detailed by *Campana* [1990, 1994]. The SW radiation parameterization scheme is based on the work of *Lacis and Hansen* [1974]. A mean cosine of the solar zenith angle, $\bar{\mu}$, is employed to calculate the SW fluxes at each model grid point, and it is computed for each model latitude as in the following equation [*Manabe and Strickler*, 1964]:

$$\bar{\mu} = \frac{\int_{\text{daylight}} \mu(t)\, dt}{\int_{\text{daylight}} dt}, \tag{1}$$

where $\mu(t)$ is the cosine of the solar zenith angle at time t. The mean cosine of the solar zenith angle is a function of latitude. The development of the longwave radiation scheme and its details are given by *Fels and Schwarzkopf* [1975] and *Schwarzkopf and Fels* [1985, 1991].

3. Adjoint Sensitivity Analysis Method

Adjoint sensitivity analysis methods have been extensively applied to initial value problems [e.g., *Hall et al.*, 1982; *Rabier et al.*, 1992; *Rabier et al.*, 1996; *Zou et al.*, 1993]. Here we deal with a radiation model. A radiation model is represented by a set of diagnostic equations. We shall develop an adjoint sensitivity analysis method applicable to radiation models. A general mathematical description of this method is provided in Appendix A.

In the present study we focus on the sensitivity of the Earth's radiation budget to changes in atmospheric moisture q, temperature T, pressure p, cloud fractions C_i ($i = 1, 2, 3$ for high, middle, and low clouds), and surface temperature T_s. The amounts of O_3 and CO_2 were not considered as variables here since these two variables are given climatological values with seasonal variations in the model. Extension to these two variables, or even to other parameters, is straightforward.

Let $F^{\uparrow}_{\text{stoa}}$ denote upward SW radiative fluxes at the top of the atmosphere, and let $F^{\uparrow}_{\text{ltoa}}$ denote outgoing longwave radiation (OLR) fluxes. We define the total absorbed shortwave radiation (ASR) by the atmosphere and Earth's surface and OLR over the global domain by

$$R_s(C_i, q, T, T_s, p) = \sum_{j=1}^{J} (\bar{S}_j^{\downarrow} - (F^{\uparrow}_{\text{stoa}})_j) = (\bar{S} - F^{\uparrow}_{\text{stoa}}) \cdot I, \tag{2}$$

$$R_l(C_i, q, T, T_s, p) = \sum_{j=1}^{J} (F^{\uparrow}_{\text{ltoa}})_j = F^{\uparrow}_{\text{ltoa}} \cdot I, \tag{3}$$

where $\bar{S}_j^{\downarrow}$ are downward day-averaged solar fluxes at the top of the atmosphere (TOA) and j stands for all horizontal model grid points defined in the radiation model. Here $\bar{S}^{\downarrow}$, $F^{\uparrow}_{\text{stoa}}$, and $F^{\uparrow}_{\text{ltoa}}$ are J-dimensional vectors, I is a J-dimensional vector of the form $(1, 1, \cdots, 1)$, and the center dot denotes the scalar product. As described in the introduction, we shall calculate the derivatives of $R_s(C_i, q, T, T_s, p)$ and $R_l(C_i, q, T, T_s, p)$ with respect to C_i, q, T, T_s and p on $J \times K$ model grid points. In adjoint sensitivity analysis, $R_s(C_i, q, T, T_s, p)$ and $R_l(C_i, q, T, T_s, p)$ are referred to as response functions.

We write the model equations for both shortwave and longwave radiation in a symbolic form:

$$F^{\uparrow}_{\text{stoa}} = F^{\uparrow}_{\text{stoa}}(C_i, q, T, T_s, p), \tag{4}$$

$$F^{\uparrow}_{\text{ltoa}} = F^{\uparrow}_{\text{ltoa}}(C_i, q, T, T_s, p). \tag{5}$$

Here q, T, and p are vectors of dimension $J \times K$, and C_i ($i = 1, 2, 3$) and T_s are J-dimensional vectors.

The linearized equations of (4) and (5) are then

$$\delta F^{\uparrow}_{\text{stoa}} = \sum_{i=1}^{3} \frac{\partial F^{\uparrow}_{\text{stoa}}}{\partial C_i} \delta C_i + \frac{\partial F^{\uparrow}_{\text{stoa}}}{\partial q} \delta q + \frac{\partial F^{\uparrow}_{\text{stoa}}}{\partial T} \delta T + \frac{\partial F^{\uparrow}_{\text{stoa}}}{\partial T_s} \delta T_s + \frac{\partial F^{\uparrow}_{\text{stoa}}}{\partial p} \delta p \tag{6}$$

$$\delta F^{\uparrow}_{\text{ltoa}} = \sum_{i=1}^{3} \frac{\partial F^{\uparrow}_{\text{ltoa}}}{\partial C_i} \delta C_i + \frac{\partial F^{\uparrow}_{\text{ltoa}}}{\partial q} \delta q + \frac{\partial F^{\uparrow}_{\text{ltoa}}}{\partial T} \delta T + \frac{\partial F^{\uparrow}_{\text{ltoa}}}{\partial T_s} \delta T_s + \frac{\partial F^{\uparrow}_{\text{ltoa}}}{\partial p} \delta p, \tag{7}$$

where the expressions of the form of $\partial F^{\uparrow}_{\text{stoa}}/\partial q$ represent the Jacobian matrices.

We take the variation of (2):

$$\delta R_s(C_i, q, T, T_s, p) = -\delta F^{\uparrow}_{\text{stoa}} \cdot I. \tag{8}$$

Substitution of (6) into (8) yields (see equation (A2) in Appendix A)

$$\delta R_s(C_i, q, T, T_s, p) = -\sum_{i=1}^{3} \left[\left(\frac{\partial F^{\uparrow}_{\text{stoa}}}{\partial C_i} \right)^T I \right] \cdot \delta C_i - \left[\left(\frac{\partial F^{\uparrow}_{\text{stoa}}}{\partial q} \right)^T I \right] \cdot \delta q - \left[\left(\frac{\partial F^{\uparrow}_{\text{stoa}}}{\partial T} \right)^T I \right] \cdot \delta T - \left[\left(\frac{\partial F^{\uparrow}_{\text{stoa}}}{\partial T_s} \right)^T I \right] \cdot \delta T_s - \left[\left(\frac{\partial F^{\uparrow}_{\text{stoa}}}{\partial p} \right)^T I \right] \cdot \delta p \tag{9}$$

where the superscript T denotes a transpose.

Thus we obtain

$$\frac{\partial R_s}{\partial C_i} = -\left(\frac{\partial F^{\uparrow}_{\text{stoa}}}{\partial C_i} \right)^T I \qquad i = 1, 2, 3 \tag{10}$$

$$\frac{\partial R_s}{\partial q} = -\left(\frac{\partial F^{\uparrow}_{\text{stoa}}}{\partial q} \right)^T I \tag{11}$$

$$\frac{\partial R_s}{\partial T} = -\left(\frac{\partial F^{\uparrow}_{\text{stoa}}}{\partial T} \right)^T I \tag{12}$$

$$\frac{\partial R_s}{\partial T_s} = -\left(\frac{\partial F^{\uparrow}_{\text{stoa}}}{\partial T_s} \right)^T I \tag{13}$$

$$\frac{\partial R_s}{\partial p} = -\left(\frac{\partial F^{\uparrow}_{\text{stoa}}}{\partial p} \right)^T I. \tag{14}$$

Here we have used the property described in (A1) in Appendix A.

Similarly, we have for $R_l(C_i, q, T, T_s, p)$

$$\frac{\partial R_l}{\partial C_i} = \left(\frac{\partial F^{\uparrow}_{\text{ltoa}}}{\partial C_i} \right)^T I \qquad i = 1, 2, 3 \tag{15}$$

$$\frac{\partial R_l}{\partial q} = \left(\frac{\partial F^{\uparrow}_{\text{ltoa}}}{\partial q} \right)^T I \tag{16}$$

$$\frac{\partial R_l}{\partial T} = \left(\frac{\partial F^{\uparrow}_{\text{ltoa}}}{\partial T} \right)^T I \tag{17}$$

$$\frac{\partial R_l}{\partial T_s} = \left(\frac{\partial F^{\uparrow}_{\text{ltoa}}}{\partial T_s} \right)^T I \tag{18}$$

$$\frac{\partial R_l}{\partial p} = \left(\frac{\partial F^{\uparrow}_{\text{ltoa}}}{\partial p} \right)^T I. \tag{19}$$

When $-I$ is viewed as a variable in (10)–(14) and I is a variable in (15)–(19), the model consisting of equations (10)–(15) is just the so-called adjoint model (see equation (A7)). We can see that the adjoint model is the transpose of linearized equations (6) and (7). A general mathematical definition of an adjoint model is given in Appendix A. Having this adjoint model at hand, we can calculate all required derivatives by one evaluation of the adjoint model. In other words, using $-I$ as an input variable of the adjoint model for the shortwave radiation part and I for the longwave radiation part, we perform one evaluation of the adjoint model. The results obtained are all required derivatives. In Appendix A we further show how the derivatives of a general response function are calculated in terms of an adjoint model.

We have derived the code of the adjoint model using the method described by *Navon et al.* [1992] and *Zou* [1997]. This method is to derive the adjoint code directly from the original nonlinear code, thus ensuring consistency of the adjoint code with the original nonlinear one. It is noteworthy that the computational effort required for the evaluation of this adjoint model is about 3 times as large as that of the original nonlinear model. This illustrates the high efficiency of sensitivity analysis using the adjoint technique.

Prior to performing adjoint sensitivity analysis, we verified the correctness of the adjoint code and assessed the range of validity of the linearization as explained in the introduction and Appendix A. Recent studies present evidence that linearizations of radiation models do work well. *Chou and Neelin* [1996] indicated that the linear scheme well reproduced the nonlinear results in simulation of LW radiative fluxes associated with interannual variability and seasonal variations in intermediate tropical atmospheric models. Diagnostic results of radiative fluxes in several sophisticated radiation models by *Zhang et al.* [1994b] also showed that nonlinear solutions display some linear properties. We shall numerically assess the range of perturbation sizes for which the linearization approximation is valid to a given tolerance.

The verification of the correctness of the adjoint code is based on the definition of adjoint equation (A2). For any given $z = (\delta C_i, \delta q, \delta T, \delta T_s, \delta p)^T$,

$$\delta F_{\text{toa}} \cdot \delta F_{\text{toa}} = z^T \cdot z^* \tag{20}$$

holds to computer precision, where F_{toa} stands for $F^{\uparrow}_{\text{stoa}}$ or $F^{\uparrow}_{\text{ltoa}}$, calculated from (6) and (7). Here $z^* = (\delta C_i, \delta q, \delta T, \delta T_s, \delta p)^T$ is calculated from (10)–(19) when I is replaced by $-\delta F_{\text{toa}}$ for (10)–(14) and δF_{toa} for (15)–(19).

Two methods are available for assessing validity of the linearization. The first one is to compare δF_{toa} from the linearized equations (6) and (7) with the nonlinear solutions of (4) and (5):

$$\Delta F_{\text{toa}} = F_{\text{toa}}(C_i + \delta C_i, q + \delta q, T + \delta T, T_s + \delta T_s, p + \delta p) - F_{\text{toa}}(C_i, q, T, T_s, p). \tag{21}$$

We calculate the correlation coefficient between δF_{toa} and ΔF_{toa}, though other quantities are available such as the rela-

Table 1. Results of the Gradient Test and Correlation Coefficients Between the Nonlinear and Linear Solutions

	Gradient Test t		Correlation Coefficients	
α	Shortwave	Longwave	Shortwave $F^{\uparrow}_{\text{stoa}}$	Longwave $F^{\uparrow}_{\text{ltoa}}$
10^{-1}	0.9981116206659	0.5373190715952	0.9998032528085	0.8918540244934
10^{-2}	1.0001212323730	0.9875666899427	0.9999843962985	0.9876367592081
10^{-3}	1.0000835059890	0.9963953949818	0.9999951542254	0.9991353107131
10^{-7}	1.0000000340750	0.9999994083835	0.9999999999999	0.9999999999986
10^{-8}	0.9999946586258	0.9999999912610	0.9999999999947	0.9999999999995
10^{-9}	0.9999968097493	0.9999953800715	0.9999999994749	0.9999999999715

The size of the atmospheric and surface perturbations is proportional to α.

tive error of the linear solution [*Li et al.*, 1993]. The second one is based on the Taylor expansion of $R(C_i, q, T, T_s, p)$:

$$R(C_i + \delta C_i, q + \delta q, T + \delta T, T_s + \delta T_s, p + \delta p) = R(C_i, q, T, T_s, p) + \nabla_{(C_i,q,T,T_s,p)}R \cdot z + \text{high-order terms}, \quad (22)$$

where $R_s(C_i, q, T, T_s, p)$ stands for $R(C_i, q, T, T_s, p)$ or $R_l(C_i, q, T, T_s, p)$. We thus design a test value

$$t = [R(C_i + \delta C_i, q + \delta q, T + \delta T, T_s + \delta T_s, p + \delta p) - R(C_i, q, T, T_s, p)] \cdot (\nabla_{(C_i,q,T,T_s,p)}R \cdot z)^{-1}, \quad (23)$$

where $\nabla_{(C_i,q,T,T_s,p)}R$ is evaluated from the adjoint equations (10)–(19). The quantity t measures the accuracy of the linearization approximation. The linearized equations (6) and (7) are consistent with the nonlinear model if t tends to 1 to computer precision as z tends to zero; in such a case, the adjoint code is also correct. Such a test process is called a gradient test [e.g., *Navon et al.*, 1992; *Li et al.*, 1993].

In all the following calculations the NCEP reanalyses are used. Table 1 presents an example of the results. In these calculations the basic state consists of the reanalyses at 0000 UT June 29, 1989. The perturbations were produced by removing part of the largest spatial scale components for wind components, temperature, pressure, and surface temperature. The sizes of perturbations are controlled by multiplying perturbations by a given constant α (when α ranges between 10^{-1} and 10^{-9}; see Table 1). Perturbed moisture and cloud fractions are obtained by simply multiplying the corresponding basic states by 3α, where 3α, rather than α, is used to account for large variabilities of moisture and cloud cover. The sizes of perturbations tend to zero when α goes to zero. From Table 1 we see that t reaches 1 to computer precision around $\alpha = 10^{-7}$ (see Appendix B), and this verifies the consistency between the linear and nonlinear models and the correctness of the adjoint.

We can also conclude that the linearization is valid for a considerable range of perturbation sizes. When $\alpha = 0.1$, the perturbations are around 4 K for temperature, 5 m/s for wind speed, 10 hPa for pressure, 4 g/kg for moisture mixed ratios, and 0.2 for cloud fraction. The linearization approximation is valid with a high degree of accuracy for SW radiation, while the

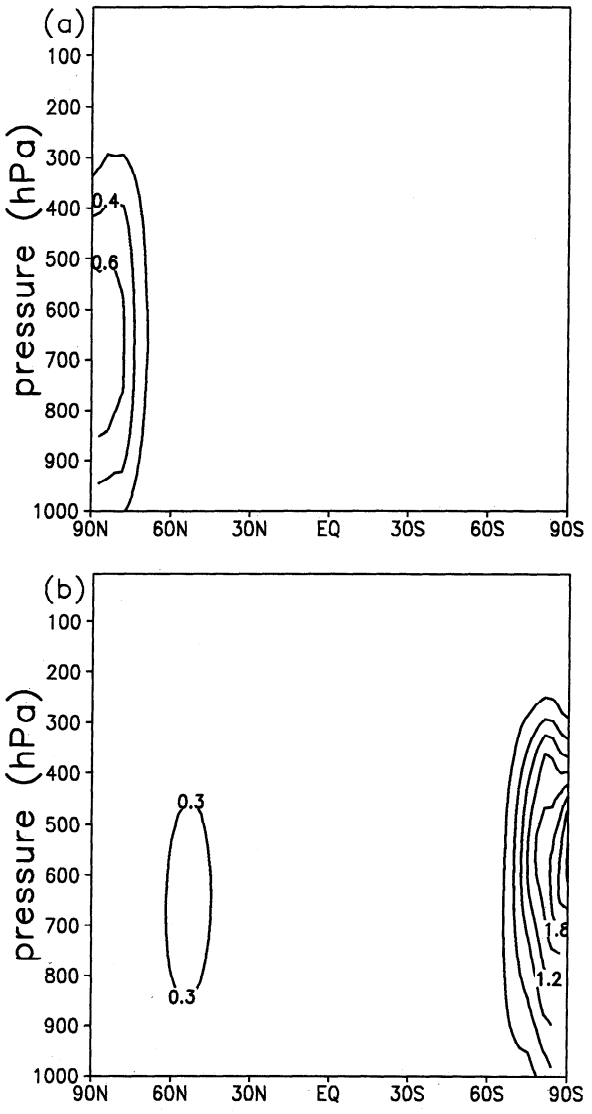

Figure 1. The zonally averaged sensitivities of the absorbed shortwave radiation (ASR) by the atmosphere and Earth's surface to water vapor mixing ratios (g kg^{-1}) for (a) June 19–29, 1989, and (b) December 19–29, 1989. The contour interval is 0.2 W m^{-2} g^{-1} kg in Figure 1a and is 0.3 in Figure 1b. In all figures, the top panel is for June 19–29, 1989, and the bottom panel is for December 19–29, 1989.

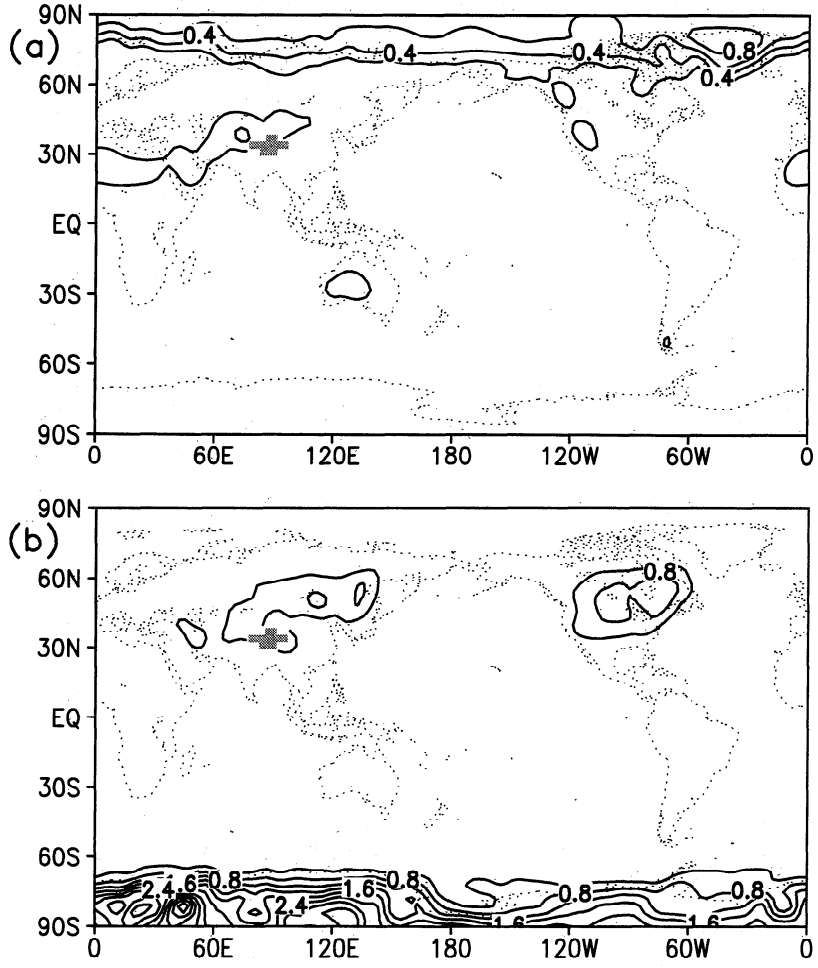

Figure 2. Same as Figure 1 but for sensitivities of the ASR to water vapor mixing ratios at 560 hPa. The contour interval is 0.2 W m^{-2} g^{-1} kg in Figure 2a and 0.4 W m^{-2} g^{-1} kg in Figure 2b. The stippled region is under the surface.

accuracy is lower but within a tolerable range for LW radiation, as indicated by a correlation coefficient as high as 0.89. This suggests that the linearization may be valid even for values of α as large as 0.1. A number of similar calculations have been carried out for different basic states representative of different months and seasons, and consistent results were obtained. Thus we conclude that the results shown in Table 1 are robust.

It is worth noting that the above conclusions are true only when the discontinuities (in both functions and the first-order derivatives) in the original radiation models are properly handled. We analyzed the impact of discontinuities on the validity of the linearization routine by routine and found that the discontinuities associated with table look-ups and cloud calculations may cause a lack of validity of the linearization; we then removed these discontinuities by replacing table look-ups and functions with discontinuities with cubic spline interpolations and sine and cosine function expansions.

4. Sensitivity Analysis

We shall present sensitivity analysis results for 0000 UT, June 19–29 and December 19–29, 1989, which are representative of the northern summer and winter seasons. Clear and cloudy skies are discussed. In cloud radiative forcing calculations, clear and cloudy skies were defined with a slight difference [*Cess and Potter*, 1987; *Zhang et al.*, 1994a]. We adopted the definition of clear sky as in so-called "method II" [*Cess and Potter*, 1987]. In this definition the states of the clear-sky atmosphere are not changed, while the clouds are set to zero.

Apart from the response functions defined in (2) and (3), we define another response function:

$$R_{\text{net}} = R_s - R_l. \tag{24}$$

R_{net} is representative of the total net ERB over the global domain. In the following, time-averaged sensitivities of atmospheric moisture, temperature, clouds and surface temperature will be discussed. The time averaging is performed by averaging daily sensitivity analysis.

4.1. Clear-Sky Case

4.1.1. Shortwave radiation sensitivity. Water vapor can absorb SW radiation [*Lacis and Hansen*, 1974]. An increase in water vapor will cause an increase in ASR. Figure 1 presents the zonally averaged sensitivity of moisture. A remarkable feature is that ASR is most sensitive to water vapor mixing ratios at high latitudes in the summertime hemisphere, while the tropics is an insensitive region.

These latitude dependent features are linked to the surface

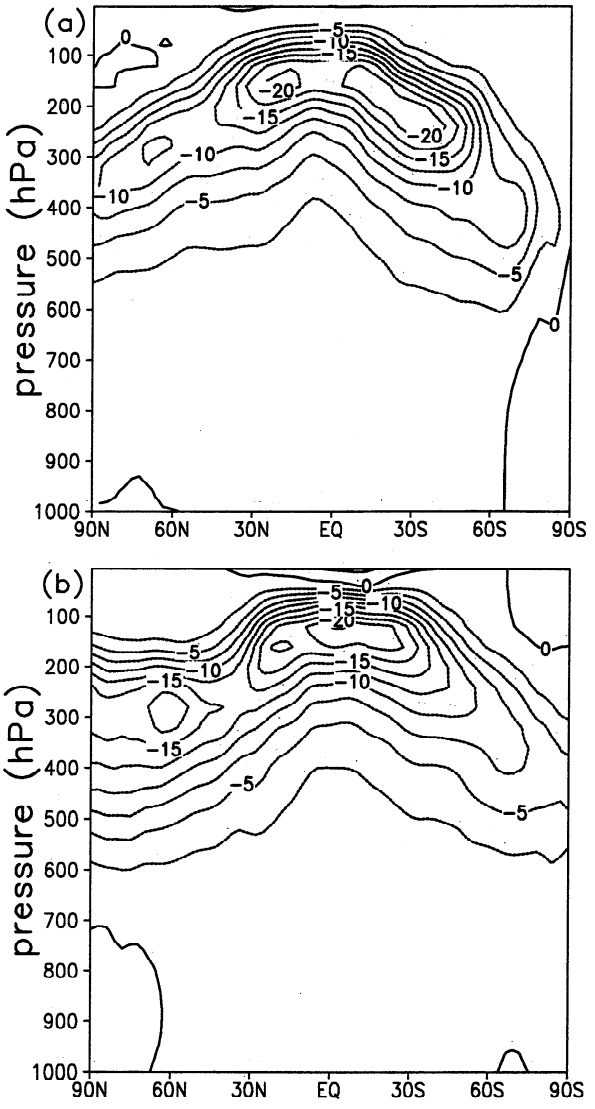

Figure 3. The zonally averaged sensitivities of the outgoing longwave radiation (OLR) at the top of the atmosphere to water vapor mixing ratios. The contour interval is 2.5 W m^{-2} g^{-1} kg. Dashed lines denote negative values.

albedo. Water vapor may have a larger absorption ratio and cause a larger atmospheric heating rate at the tropics due to stronger incident solar radiation. Since the tropical surface is characterized by oceans with large darkness (near black bodies), the atmosphere and surface system almost fully absorb the incident radiation, irrespective of the absorption by water vapor. Thus the absorption by water vapor has little effect on ASR. By contrast, the surface at high latitudes is characterized by snow or ice cover with large brightness, the absorption by water vapor being nearly equal to the net increase in ASR. The sensitivity structure at 600 hPa (Figure 2), which corresponds to the maximum absorption height, illustrates the predominant linkage to the surface albedo; i.e., we can see a larger sensitivity over the summer polar areas and lands with larger albedo. We observe that the sensitivity structures are rather symmetric about the equator between the northern and southern summertime, though the sensitivity at high latitudes in the southern summer hemisphere is stronger than that in the northern summer hemisphere.

4.1.2. Longwave radiation sensitivity. OLR strongly depends on water vapor amount and its spatial distribution and on the AES temperature features. The vertical structure of the atmospheric temperature strongly affects OLR variations.

Figure 3 illustrates the zonally averaged sensitivity structure of the moisture for OLR. A striking feature is the larger sensitivity found near the tropopause, with a maximum of 22 W m^{-2} g^{-1} kg. The middle and lower troposphere have a magnitude of less than 2.5 W m^{-2} g^{-1} kg. On the whole, OLR is 1 order of magnitude more sensitive to the mixing ratio in the upper troposphere than in the middle and lower troposphere. The high sensitivity of OLR to the water vapor in the upper troposphere has been noted in observational studies. *Kiehl and Briegleb* [1992] indicate that the differences in upper tropospheric moisture are the major cause for the OLR difference during a 2-year observation period in most regions over the tropical oceans. This result may be helpful for understanding the super greenhouse effect over tropical oceans, which will be discussed in the following section.

Some meridional features in Figure 3 are also of interest. In the middle and lower troposphere, sensitivities have a small

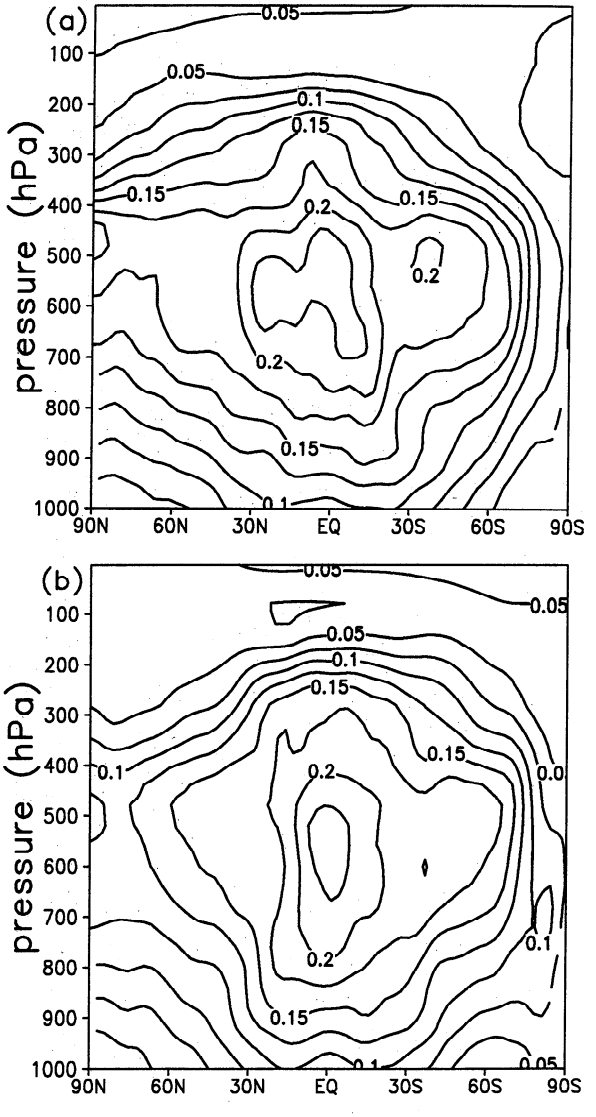

Figure 4. Same as in Figure 3 but for atmospheric temperature. The contour interval is 0.025 W m^{-2} K^{-1}.

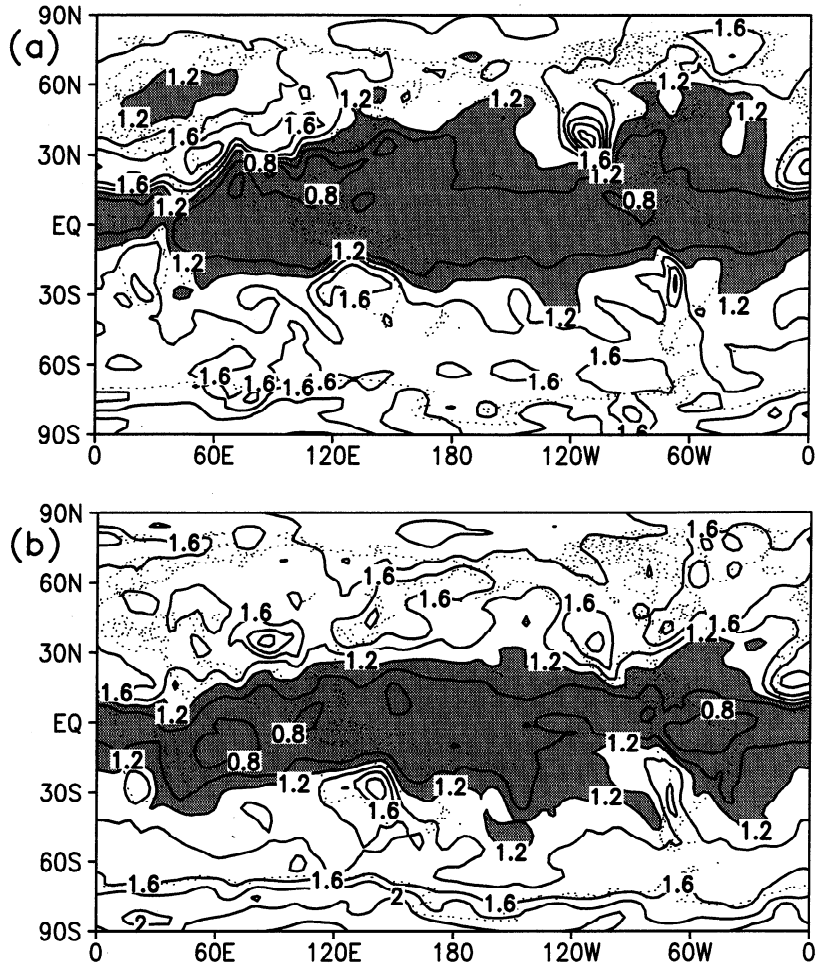

Figure 5. Sensitivities of the OLR to the Earth's surface temperature. The contour interval is 0.25 W m^{-2} K^{-1}. Stippled regions denote sensitivities smaller than 1.2 W m^{-2} K^{-1}.

positive value at the high latitudes, while the positive value is slightly larger in the winter hemisphere than in the summer hemisphere. Near the tropopause, sensitivities are relatively large between the subtropics of the summer hemisphere and the middle latitude of the winter hemisphere. The existence of two weak sensitivity regions at latitudes of around 30°N in the northern winter and 45°N in the northern summer are of interest. These two regions are linked to activities of polar fronts [*Palmén and Newton*, 1967].

Qualitatively, we can understand these results by considering the radiation transfer equation. We may write the perturbed radiation transfer equation as [*Stephens*, 1984]

$$F'^{\uparrow}_{\text{ltoa}} = -\int_0^{\infty}\int_0^{\infty} \tau'_{\nu}(z, h)\,\frac{dB_{\nu}(h)}{dh}\,dh\,d\nu, \qquad (25)$$

where ν is wavenumber, B_{ν} is the Planck function, $F'^{\uparrow}_{\text{ltoa}}$ is the perturbed OLR flux associated with water vapor perturbations, and $\tau'_{\nu}(z, h)$ is the perturbed transmission function between levels h and z. B_{ν} is a function of the temperature T, and thus $dB_{\nu}(h)/dh$ depends on temperature lapse rates. A large temperature lapse rate leads to a large magnitude of perturbed OLR. The inversion enhances OLR, which is the leading cause of positive values of sensitivities at high latitudes.

The sensitivity of atmospheric temperature displays a strong spatial variation (Figure 4). In the vertical the largest sensitivities are located between 600 and 500 hPa, and the globally averaged sensitivity at 600 hPa is about 0.2 W m^{-2} K^{-1}. The sensitivities rapidly decrease above and below the largest sensitivity regions. The sensitivity between 600 and 500 hPa is 1 order of magnitude larger than that near the tropopause and 3 times stronger than that near the surface. As far as the latitudinal variation is concerned, the sensitivities are largest over tropical areas and decrease toward the poles. Unlike water vapor, the sensitivity structure of the atmospheric temperature does not present a significant difference between the northern summer and southern summer. It is worth noting that a 1-K temperature perturbation in the middle troposphere produces an OLR increase equivalent to that produced by a 0.1 g/kg water vapor perturbation in the middle and lower troposphere or by a perturbation of about 0.15 K in the surface temperatures (see the following discussion). Thus temperature perturbations in the middle troposphere exert a significant effect on OLR variabilities.

Figure 5 shows the sensitivity structures of the surface temperature. A positive surface temperature perturbation results in an increase in the emission of LW radiation and thus an increase in OLR when feedbacks are not taken into account (an increase in sea surface temperatures may lead to a decrease in OLR when the feedback of water vapor is involved

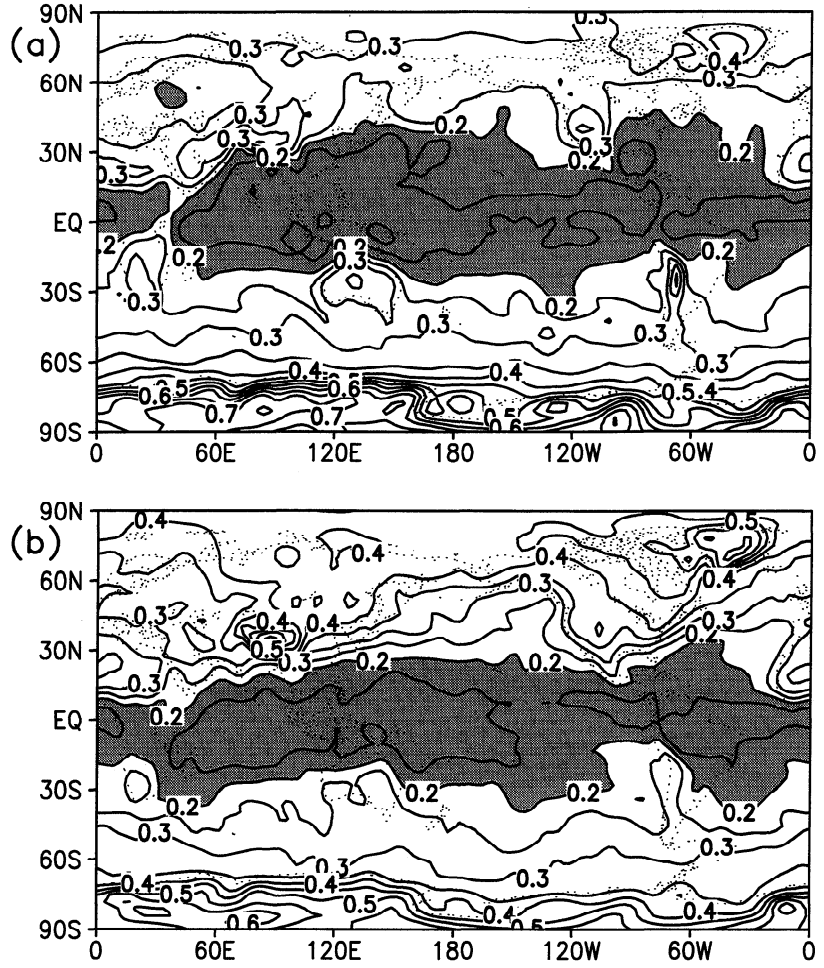

Figure 6. Sensitivities of the OLR to the Earth's surface perturbation emission. These sensitivities are the ratios between an increase in the Earth's surface emission and the corresponding increase in OLR. The contour interval is 0.05. Stippled regions denote ratios larger than 0.2 or indicate that atmospheric columns trap more than 80% of a perturbation increase in the Earth's surface emission.

[*Inamdar and Ramanathan*, 1994]). The globally averaged sensitivity is 1.4 W m^{-2} K^{-1}. As expected, the tropical areas display the smallest sensitivities due to the strong greenhouse trapping by abundant water vapor. On the average, the tropical sensitivities are about half as large as those at middle and high latitudes. The sensitivities tend to increase from the tropics to the polar regions. However, this increase with latitude is not uniform, and we observe rapidly decreasing bands in the subtropical regions. Such a meridional variation is especially obvious in the northern winter hemisphere. The regions of weak sensitivity over the tropical oceans are consistent with regions of large greenhouse trapping observed in the ERBE [e.g., *Raval and Ramanathan*, 1989; *Kiehl and Briegleb*, 1992]. There are some other minor features. The regions of high orography, for instance, the Tibetan Plateau and the Rocky Mountains, are characterized by large sensitivities. North Africa and part of Australia are relatively sensitive regions, which is a consequence of their drier atmosphere. The northeastern regions of the Pacific and Atlantic Oceans, which are associated with the upward motion in the front of the semipermanent troughs over the central oceans, are relatively insensitive [*Palmén and Newton*, 1967].

To describe the greenhouse trapping, we analyzed the sensitivity of the surface LW emission. The gradients of the response R_l with respect to the surface emission, $\nabla_{se}R_l$, are not a direct output variable of the adjoint model but can be obtained from $\nabla_{T_s}R_l$:

$$\nabla_{se}R_l = \frac{\nabla_{T_s}R_l}{4\sigma T_s^3}, \tag{26}$$

where $\nabla_{T_s}R_l$ is the gradient of R_l with respect to the surface temperatures T_s and σ is the Stefan-Boltzmann constant. The magnitude of $\nabla_{se}R_l$ actually represents the factor of the perturbed OLR, which varies between 0 and 1. An increased perturbation emission at the surface is completely trapped by the column atmosphere when the gradient is 0 and escapes completely out of the top of the atmosphere when the gradient is 1. Figure 6 illustrates the structure of $\nabla_{se}R_l$. We observe that less than 20% of an increased perturbation emission at the surface goes out of the top of the atmosphere over the tropical areas. In other words, the column tropical atmosphere traps more than 80% of a perturbation increase in the emission at the surface. The magnitude of $\nabla_{se}R_l$ at midlatitudes is, in general, larger than 30%, while at high latitudes it is larger than 40%. It has long been found that the moistening effect of deep convection activity strongly enhances the atmospheric greenhouse effect [e.g., *Raval and Ramanathan*, 1989]. In our calculations the regions with a greenhouse trapping larger than

80% significantly correlate with deep convection activities. Analysis showed that this is also the case for the region within the inner Eurasian continent in northern summer. It is of interest to note that the deep upward motion in the front of the semipermanent troughs over the middle Pacific and Atlantic Oceans in the wintertime may play a role similar to deep convective activities, and the greenhouse trapping is about 70–80% over these areas.

4.2. Cloudy-Sky Case

The interaction between radiation and clouds has long presented a fundamental challenge. In atmospheric general circulations models the representation of this interaction has undergone a considerable improvement during recent years, but substantial deficiencies are still present, as indicated by model comparisons [*Cess et al.*, 1996]. The interaction comprises two processes: Clouds affect radiation by absorption and reflection, and radiation affects clouds through changing the structure of the atmosphere by heating and cooling. The first aspect is generally thought to be easily depicted in the model. Unfortunately, its depiction is by far unsatisfactory [*Baer et al.*, 1996; *Ellingson and Fouquart*, 1991]. The following analysis intends to show the effects of variations in cloud fraction on the ASR and OLR.

4.2.1. Shortwave radiation sensitivity. Figure 7 presents the zonally averaged sensitivity structure of clouds for SW radiation. In this adjoint sensitivity analysis we compute the sensitivity only for the regions where clouds are present in the basic states.

The cloud reflection effect on SW radiation is characterized by negative sensitivity. The sensitivity has a tendency to proportionally increase with the incident solar radiation, but there are important features that result from atmospheric variations. ASR is most sensitive to low clouds; this result may primarily be a consequence of assigning a larger reflectivity to low clouds. The high latitudes in both the wintertime and summertime hemispheres are extremely insensitive regions. The high albedo of the surface in these regions is responsible for this super insensitivity, since an increase in cloud fractions has little additional reflective effect on ASR over snow and ice at high latitudes. Three types of clouds present different meridional variations. In order to illustrate this point we provide the latitudinal variations of sensitivity of the three types of clouds (same as defined in the model) (Figure 8). In the wintertime hemispheres the sensitivity of the three types of clouds consistently increases from zero at high latitudes to about 20 W m^{-2} for a 0.1 cloud fraction increase at the equator, and the low clouds have a slightly larger sensitivity. While the high clouds are most sensitive at the latitude consistent with the location of the largest incident solar radiation, the low clouds tend to have the largest sensitivity at midlatitudes in the summertime hemisphere. Consequently, the difference between the high and low clouds reaches its maximum at summer middle latitudes, and the low cloud sensitivity is on the average about 30 W m^{-2} per 0.1 cloud fraction in these latitudes. This sensitivity is twice as large as that of the high clouds, which is about 15 W m^{-2} per 0.1 cloud fraction.

4.2.2. Longwave radiation sensitivity. Figure 9 shows the zonally averaged sensitivity structure of clouds for LW radiation. The effects of clouds on OLR are similar to the effects of water vapor and are intimately related to temperature lapse rates. The largest sensitivity is located near the tropopause and at the tropics, with a shift of about 10° to the summertime

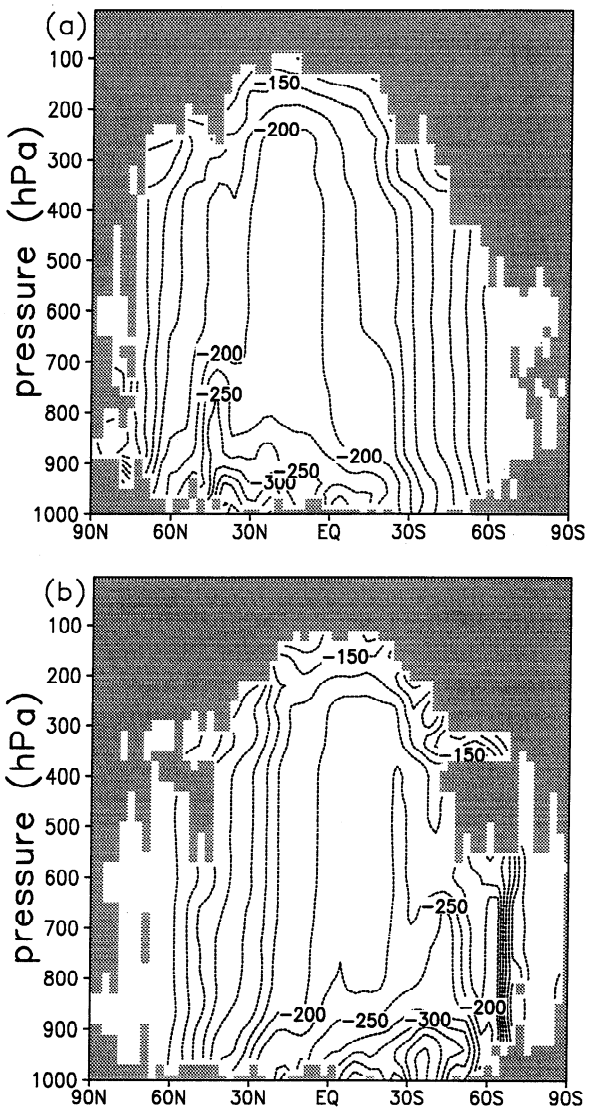

Figure 7. The zonally averaged sensitivities of the ASR. The contour interval is 50 W m^{-2} per cloud fraction, i.e., equivalent to an increase of 5 W m^{-2} in the ASR due to a 0.1 cloud fraction increase. Regions without clouds in the basic states are stippled, where sensitivities are not calculated.

hemispheres. Associated with the inversion at the polar latitude, the sensitivity has a small positive value. The rates of vertical decrease in the sensitivities are largest between 900 and 700 hPa. This feature indicates that the OLR is more sensitive to the high and middle clouds than to low clouds. To further illustrate this feature, we also depicted the sensitivity variation of the three types of clouds with latitude (Figure 10). The sensitivity to high and low clouds displays a consistent meridional variation, whereas low clouds present a significantly smaller sensitivity apart from the high latitudes. At the tropics the sensitivities of the middle and high clouds are on the average about 11 W m^{-2} per 0.1 cloud fraction, which is twice as large as that of the low clouds. At high latitudes the sensitivity of all three types of clouds becomes smaller, attaining even smaller positive values at polar latitudes. This feature is evident in observations by *Yamanouchi and Charlock* [1995].

4.2.3. Net Earth radiation budget sensitivity. The sensitivity of the net ERB to clouds is closely related to cloud

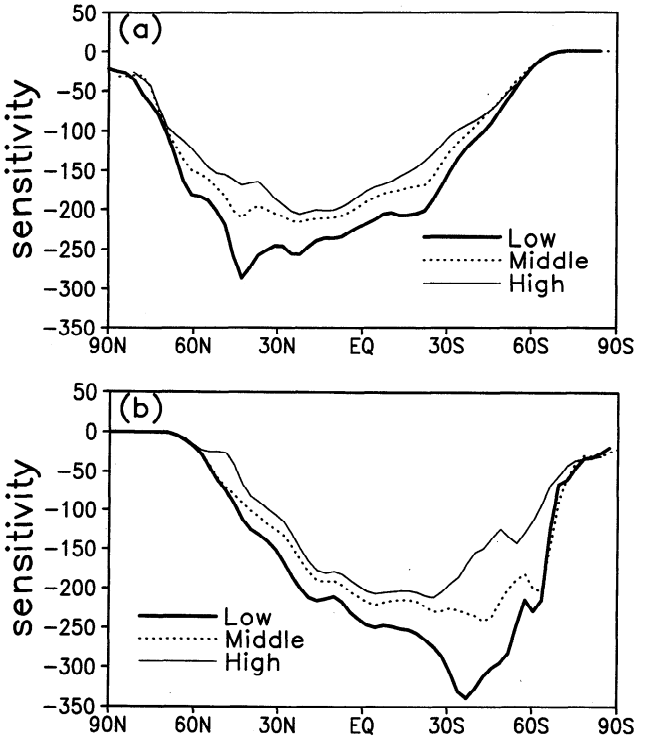

Figure 8. The zonally averaged sensitivities of the ASR to three types of clouds (high, middle, and low). The unit is W m^{-2} per cloud fraction.

radiative forcing. Figure 11 illustrates the zonally averaged sensitivity structure. There are two striking features: a cancellation occurring between the LW greenhouse effect and the SW reflection for middle and high clouds at lower latitudes, and a strong negative sensitivity of low clouds at the summer midlatitudes. These two features are evident when we carry out a comparison between the sensitivity structures of SW and LW radiation in Figures 7 and 9. The middle and high clouds at lower latitudes strongly trap the LW radiation and simultaneously strongly reflect the SW radiation. Thus a large cancellation occurs in the middle and high cloud areas at lower latitudes. The low clouds cause a smaller LW trapping but a larger SW reflection. Such an opposite tendency creates a larger positive sensitivity to low clouds. We emphasize the importance of low clouds at the summer midlatitudes, i.e., where the net ERB displays the strongest sensitivities to low clouds. This latitudinal dependence is consistent with observed results that the net cloud cooling effect on the Earth is larger over the middle and high latitude oceans [e.g., *Ramanathan et al.*, 1989]. Such features are evident in the sensitivity variations of the three types of clouds with latitude (Figure 12). The low clouds, especially at midlatitudes, may play a role in the Earth's radiation budget variations.

At the tropics, observations [e.g., *Ramanathan et al.*, 1989] from ERBE show that the LW cloud forcing and the SW cloud forcing are nearly canceling each other in tropical convective regions. Our calculations (Figure 11) showed that even near the top of clouds at about 200 hPa the SW cloud forcing is larger than the LW cloud forcing, while the low clouds produce a much stronger SW forcing than the LW forcing. This result is not consistent with the observations. *Campana* [1994] and *Yang et al.* [1995] have found an overestimation of the cloud SW reflection in this model, and this deficiency has been reduced in the updated version [*Hou et al.*, 1996]. The inconsistency may be partly due to this overestimation. There are two other possible factors that may contribute to this inconsistency: First, the observations may overestimate the LW cloud forcing [*Inamdar and Ramanathan*, 1994; *Kiehl and Briegleb*, 1992], and second, the model cloud heights are not high enough, as shown by *Kiehl* [1994], who found that a cloud top height of about 16 km is required for near cancellation of the LW and SW cloud forcing.

5. Summary and Discussion

In this study we have introduced the adjoint technique to carry out a sensitivity analysis of the Earth's radiation budget. This method efficiently calculates the partial derivatives of response functions of the Earth's radiation budget with respect to the amount of atmospheric constituents as well as the atmospheric and Earth surface states. Since the magnitudes of partial derivatives directly account for sensitivity, their fields define sensitivity structures, which allow us to investigate spa-

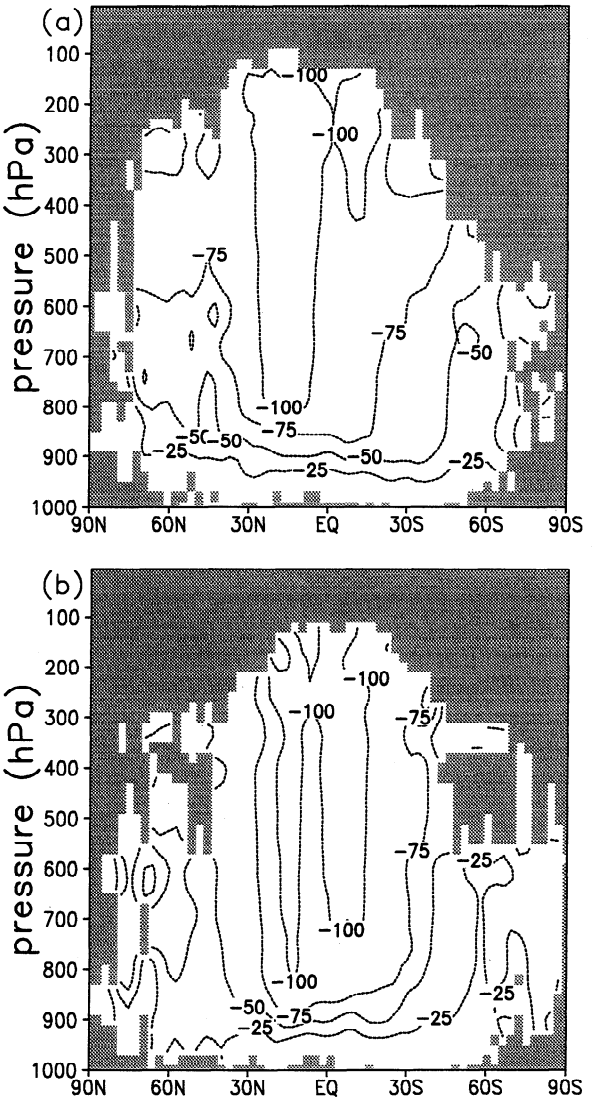

Figure 9. Same as in Figure 7 but for the OLR and with a contour interval of 25 W m^{-2}.

tial patterns of sensitivity variations. We can also estimate the relative sensitivity among various variables based on the magnitudes of partial derivatives.

We computed the partial derivatives of a defined response function with respect to all the variables on each model grid point by a single calculation of the adjoint model. Compared with the currently used direct sensitivity analysis method, the adjoint technique renders a sensitivity analysis method computationally efficient, thus allowing us to investigate sensitivity in detail. While direct sensitivity analysis is carried out for finite perturbations, the sensitivity defined by partial derivatives is theoretically valid for infinitely small perturbations. If radiation processes were linear, these two methods would be consistent. The strong nonlinearity of radiation processes may result in inconsistency. The calculations in the present study showed that the nonlinearity may not cause significant problems when cloud fraction perturbations are smaller than 0.2, water vapor mixing ratios are smaller than 4 g/kg, and the surface temperatures are smaller than 4 K. For larger perturbations, caution is required when interpreting adjoint sensitivities. In a simpler radiation model the linearization may still be valid for larger perturbations [*Chou and Neelin*, 1996].

The calculation results in this study pointed to significant spatial variations of the sensitivities. For the absorbed SW radiation (ASR) the most sensitive regions of water vapor mixing ratios were located at summer high latitudes, while the tropics was an insensitive region. Such a meridional variation in the sensitivities was primarily determined by the albedo of the surface. ASR was found to be more sensitive to low clouds than to middle and high clouds, and the most sensitive low clouds tend to be located at midlatitudes.

The OLR were found to be most sensitive to the water vapor mixing ratios near the tropopause, roughly about 20 times more sensitive than those in the lower and middle troposphere.

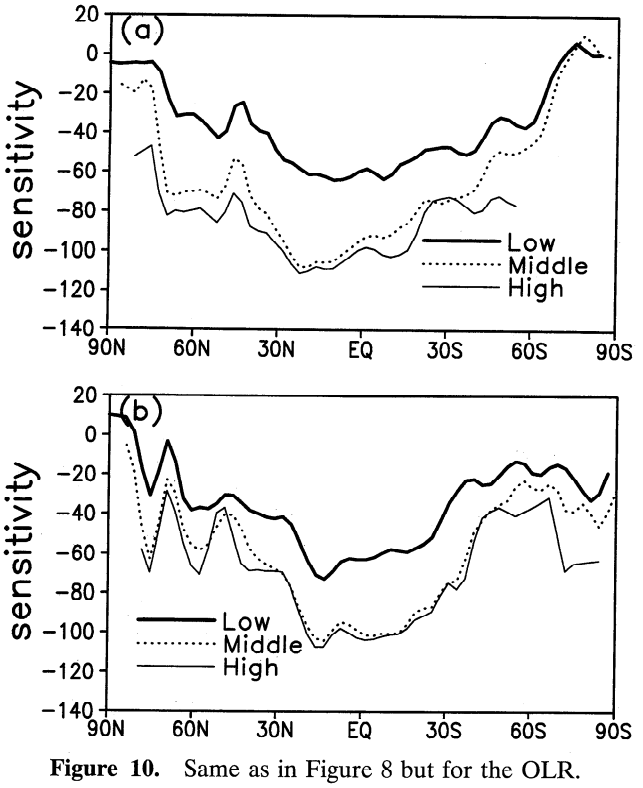

Figure 10. Same as in Figure 8 but for the OLR.

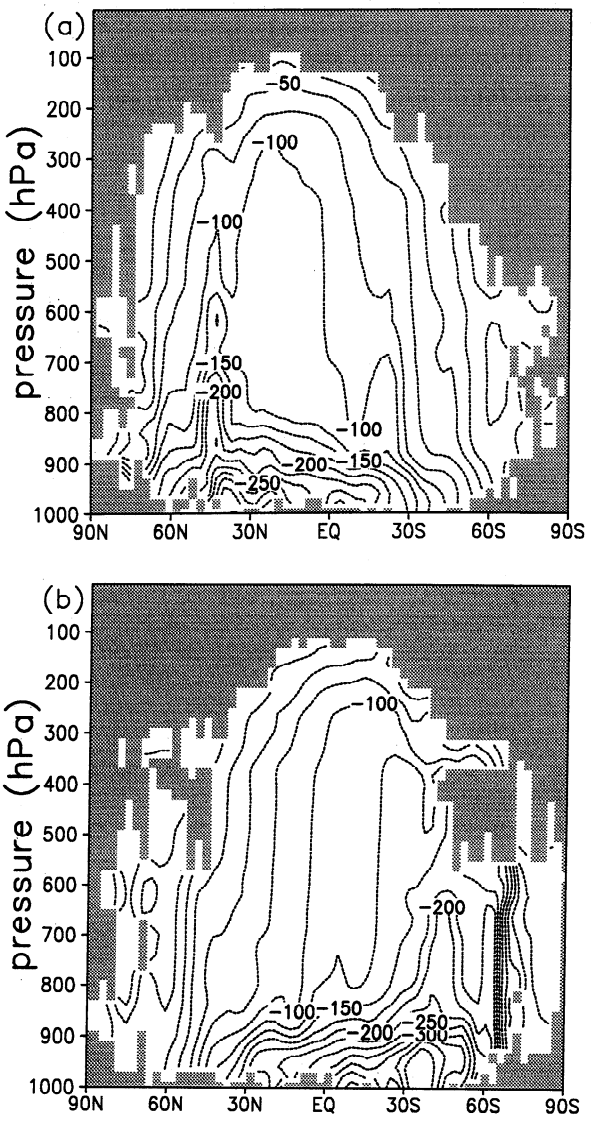

Figure 11. Same as in Figure 8 but for the zonally averaged sensitivities of the net Earth radiation budget to clouds. The negative values indicate a net decrease in the net Earth radiation with cloud increase.

The OLR was also sensitive to temperature variabilities in the middle troposphere, as illustrated by the fact that the OLR variation produced by a 1-K temperature perturbation was equivalent to that produced by a 0.1 g/kg water vapor perturbation. OLR displayed similar sensitivities to middle and high clouds but much weaker sensitivities to low clouds. The sensitivities of the middle and high clouds were on the average twice as large as those of the low clouds at lower latitudes, while the sensitivity of the three types of clouds decreased rapidly at midlatitudes.

The clear-sky atmosphere displayed the strongest LW greenhouse trapping at the tropics, with more than 80% of a perturbation increase in the Earth's surface emission being trapped. Rapidly decreasing latitude bands of the trapping were found within the subtropics, and about 60–70% of a perturbation increase in the Earth's surface emission was trapped at middle and high latitudes. The insensitivity to changes in the surface emission at the tropics could be understood by the fact that deep convection moistening effects

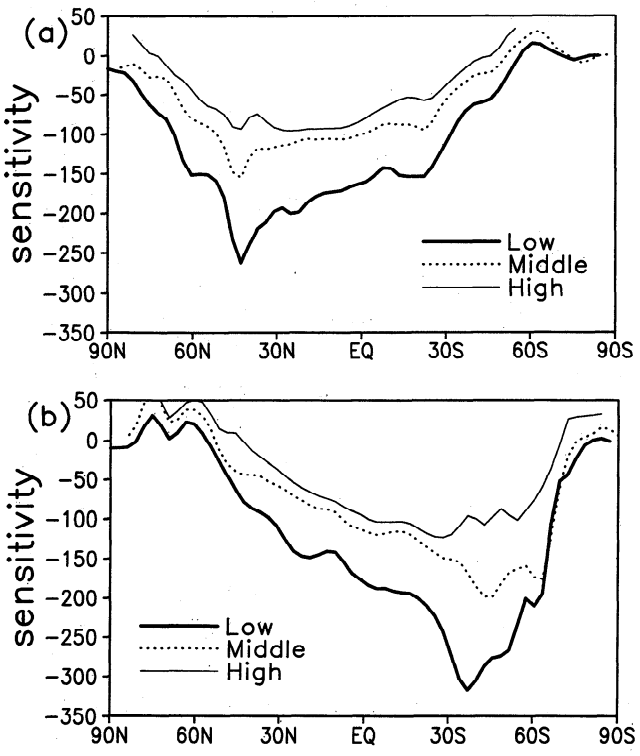

Figure 12. Same as in Figure 9 but for the sensitivity of the net Earth radiation budget to three types of clouds (high, middle, and low).

strongly enhance greenhouse effects [e.g., *Inamdar and Ramanathan*, 1994; *Kiehl and Briegleb*, 1992]. Such deep convection effects were also observed at the summer northern midlatitudes where convective activities prevail. The deep upward motion in the front of the semipermanent troughs over the central Pacific and Atlantic Oceans in the wintertime had a moistening effect similar to deep convective activities and enhanced the LW greenhouse trapping in these areas.

An increase in cloud fraction led to an decrease in the net Earth radiation budget (ERB) apart from the low and middle troposphere at polar latitudes where an inversion exists. The net ERB was found to be more sensitive to low clouds. This resulted from a stronger sensitivity of ASR and a weaker sensitivity of OLR. The net ERB was especially sensitive to summer midlatitude low clouds, with a sensitivity of 30 W m^{-2} per 0.1 cloud fraction.

Our results showed that clouds had negative sensitivities for the radiation budget; i.e., an increase in cloud fraction caused a net radiation loss except at polar latitudes, which reflects the fact that cloud forcing yielded a net cooling [e.g., *Ramanathan et al.*, 1989; *Harrison et al.*, 1990]. A more interesting result was that low clouds had larger sensitivities for ASR as well as for the net ERB. This sensitivity analysis also suggested that summer midlatitude low clouds had the largest sensitivity. These results imply that the feedback of radiation is not only affected by the change in cloud fraction but also by the change in cloud heights and geographic positions and should be further investigated.

We emphasize that our results depend on the model used, and we do not think that the results obtained directly explain the behavior of the real atmosphere. Our primary purpose is to emphasize the importance of the concept of adjoint sensitivity and especially the spatial patterns of sensitivities for an in-depth analysis of interactions between radiation and other atmospheric processes in radiation models leading to identification of model deficiencies. In order for our conclusions to reliably explain the real atmospheric processes our results must be compared with those obtained from other models as well as with those derived from observations such as data from the Atmospheric Radiation Measurement Program [*Stokes and Schwartz*, 1994]. Such comparisons will be the focus of our next research effort.

Appendix A: Description of Adjoint Sensitivity Analysis

The general theory of adjoint equations and their applications to sensitivity studies are given by *Cacuci* [1981, 1987], *Talagrand and Courtier* [1987], and *Le Dimet et al.* [1997]. To introduce this method, we will use two basic properties of Hilbert space.

1. Let $\mathcal{H}$ be a Hilbert space, with inner product denoted by parentheses, and let $R(x)$ be a scalar function defined on $\mathcal{H}$. The differential δR of R can be uniquely determined in terms of the differential δx of $x \in \mathcal{H}$ by the inner product

$$\delta R = (\nabla_x R, \delta x), \tag{A1}$$

where $\nabla_x R$ is the gradient of R with respect to x.

2. Let $\mathcal{L}$ be another Hilbert space, with inner product denoted by angle brackets, and let L be a continuous linear operator from $\mathcal{L}$ into $\mathcal{H}$. There exists a unique continuous linear operator L^* from $\mathcal{H}$ into $\mathcal{L}$, which satisfies

$$(x, Lf) = \langle L^* x, f \rangle \qquad f \in \mathcal{L} \tag{A2}$$

The operator L^* is called the adjoint of L.

When $\mathcal{H}$ and $\mathcal{L}$ are finite dimensional and represented by orthonormal coordinates, L becomes a matrix, and x and f are vectors. Further, if these two inner products are defined as the scalar product, then the components of $\nabla_x R$ are the partial derivatives $\partial R/\partial x$; the adjoint operator L^* becomes L^T, the transpose of the operator L. Here we consider such a case.

Conceptually, a radiation model may be written as

$$f = F(x), \tag{A3}$$

where f, defined on $\mathcal{L}$, may consist of radiation fluxes and radiative heating rates, and the quantities describing the atmospheric and Earth's surface states constitute x, defined on $\mathcal{H}$.

Define a response function

$$R = H(f). \tag{A4}$$

The response R may have various physical meanings depending on a suitable choice of the function H. For example, the response functions defined by (2) and (3) are representative of the total ASR and OLR at the TOA over the global domain.

The sensitivity of the response function to variations in the model variables is mathematically defined as [see *Cacuci*, 1981]

$$\delta R = H(f + \delta f) - H(f) = H'(f) \cdot \delta f, \tag{A5}$$

where $H'(f)$ is the partial derivative of H with respect to f. Here δR represents a measurement of the sensitivity of the response R to the perturbation δf.

We now introduce a linearization of (A3)

$$\delta f = L\,\delta x, \tag{A6}$$

where $L = \partial F/\partial x$ is the Jacobian matrix. The corresponding adjoint equation of (A6) is

$$\delta x^* = L^T \delta f^*, \tag{A7}$$

where δx^* and δf^* are called adjoint variables and have the same dimension as δx and δf, respectively.

Substituting (A6) into (A5) and following (A2), we obtain

$$\delta R = H'(f) \cdot L\,\delta x = L^T H'(f) \cdot \delta x \tag{A8}$$

Comparing (A8) with (A1), we then have the gradient of R with respect to x:

$$\lim_{\Delta x \to 0} \frac{\Delta R}{\Delta x} = \nabla_x R = L^T H'(f). \tag{A9}$$

Equation (A9) provides the expression of the gradient $\nabla_x R$, and it also provides a powerful method for evaluating the gradient $\nabla_x R$. It indicates that $\nabla_x R$ is just the solution of the adjoint model (A7), while $H'(f)$ is the model input. Generally, H is an explicitly defined function, and $H'(f)$ can be obtained analytically. We then can simply calculate $\nabla_x R$ by one evaluation of the adjoint model (A7).

For a finite perturbation Δx, we can obtain the approximation of the defined sensitivity using the first-order Taylor expansion:

$$\Delta R \approx L^T H'(f) \cdot \Delta x. \tag{A10}$$

By definition, a change δx in the AES states will lead to a change in the radiation response δR. From (A8) we can immediately conclude that $|\delta R|$ attains its maximum for all δx with a prescribed norm when δx is parallel to $\nabla_x R$. In other words, in regions where the gradient $\nabla_x R$ is large, a change in the atmospheric and Earth surface states would give rise to a large change in the radiation response; in regions where the gradient $\nabla_x R$ is small, a change in the AES states would affect the radiation response very little. Consequently, the pattern of the gradient $\nabla_x R$ defines the desired sensitivity structure of perturbations of the AES states. To conform to the discussion in the introduction, we refer to the components of $\nabla_x R$ as sensitivities.

It is noteworthy that the evaluated gradients of R are accurate, and their accuracy is not related to the linearization approximation. However, as mentioned in the introduction, we need to evaluate $\Delta R/\Delta x$. Since radiative processes are characterized by strong nonlinearity, (A10) is valid only in the limit of small Δx. We must provide an estimate of the size of Δx which ensures validity of (A10).

Appendix B: Validity of the Linearization

For a function $y(z)$ with continuous second derivatives, the Taylor expansion around z yields

$$y(z + \delta z) = y(z) + y'(z)\delta z + \tfrac{1}{2} y''(\xi)(\delta z)^2, \tag{B1}$$

where ξ lies between z and $z + \delta z$.

Equation (B1) may be written as

$$\frac{y(z + \delta z) - y(z)}{y'(z)\delta z} = 1 + \varepsilon \tag{B2}$$

where

$$\varepsilon = \frac{y''(\xi)\delta z}{2y'(z)} \tag{B3}$$

Note that $1 + \varepsilon$ is corresponding to t in the body of the paper. For a double precision computer machine (15-digit precision), ε is determined by (B3) when $|y''(\xi)\delta z^2/2y(z)|$ is larger than 10^{-15}. In such a case, ε is of the same order of magnitude as δz when $y''(\xi)$ and $y'(z)$ are of the same order of magnitude. Otherwise, ε is determined by $10^{-15}/y'(z)\delta z$. From the above discussions one draws the conclusion that ε attains its smallest magnitude with an order of magnitude between 10^{-7} and 10^{-8}. From this conclusion and Table 1 we obtain that the linearized and adjoint models are fully consistent with the original nonlinear model.

Acknowledgments. We thank K. A. Campana and J. Sela for their encouragement and invaluable suggestions. We are especially indebted to K. A. Campana and S.-K. Yang for valuable comments and helpful discussions. We also thank two anonymous reviewers for their insightful comments, which substantially improved this paper. This research was supported by NSF grant ATM-9413050, managed by Pamela Stephens, whom we would like to thank for her support, and by the Supercomputer Computations Research Institute, which is partially funded by the Department of Energy through contract DE-FG05-85ER250000.

References

Baer, F., N. Arsky, J. J. Charney, and R. G. Ellingson, Intercomparison of heating rates generated by global climate model longwave radiation codes, *J. Geophys. Res.*, *101*, 26,589–26,603, 1996.

Barkstrom, B. R., The Earth Radiation Budget Experiment (ERBE), *Bull. Am. Meteorol. Soc.*, *65*, 1170–1185, 1984.

Barkstrom, B. R., and G. L. Smith, The Earth Radiation Budget Experiment: Science and implementation, *Rev. Geophys.*, *24*, 379–390, 1986.

Cacuci, D. G., Sensitivity theory for nonlinear systems, I, Nonlinear functional analysis approach, *J. Math. Phys.*, *22*, 2794–2802, 1981.

Cacuci, D. G., The forward and adjoint methods of sensitivity analysis, in *Uncertainty Analysis*, edited by Y. Ronen, pp. 71–144, CRC Press, Boca Raton, Fla., 1987.

Campana, K. A., Radiation and cloud parameterization at the National Meteorological Center, in *ECMWF/WCRP Workshop on Clouds, Radiation, and the Hydrological Cycle*, pp. 313–340, Eur. Cent. for Med. Range Weather Forecasting, Reading, England, 1990.

Campana, K. A., Use of cloud analyses to validate and improve model-diagnostic clouds at NMC, in *ECMWF/WCRP Workshop on Modelling, Validation and Assimilation of Clouds*, pp. 207–231, Eur. Cent. for Med. Range Weather Forecasting, Reading, England, 1994.

Cess, R. D., and G. L. Potter, Exploratory studies of the cloud radiative forcing with a general circulation model, *Tellus, Ser. A*, *39*, 460–473, 1987.

Cess, R. D., et al., Intercomparison and interpretation of climate feedback processes in 19 atmospheric general circulation models, *J. Geophys. Res.*, *95*, 16,601–16,615, 1990.

Cess, R. D., et al., Cloud feedback in atmospheric general circulation models: An update, *J. Geophys. Res.*, *101*, 12,791–12,794, 1996.

Chou, C., and J. D. Neelin, Linearization of a longwave radiation scheme for intermediate tropical atmospheric models, *J. Geophys. Res.*, *101*, 15,129–15,145, 1996.

Ellingson, R. G., and Y. Fouquart, The intercomparison of radiation codes in climate models: An overview, *J. Geophys. Res.*, *96*, 8925–8927, 1991.

Fels, B. S., and M. D. Schwarzkopf, The simplified exchange approximation—A new method for radiative transfer calculation, *J. Atmos. Sci.*, *32*, 1475–1488, 1975.

Hall, M. C. G., D. G. Cacuci, and M. E. Schlesinger, Sensitivity analysis of a radiative-convective model by the adjoint method, *J. Atmos. Sci.*, *39*, 2038–2050, 1982.

Harrison, E. F., P. Minnis, B. R. Barkstrom, V. Ramanathan, R. D. Cess, and G. G. Gibson, Seasonal variation of cloud radiative forcing

derive from the Earth Radiation Budget Experiment, *J. Geophys. Res.*, *95*, 18,687–18,703, 1990.

Hartmann, D. L., and D. Doelling, On the net radiative effectiveness of clouds, *J. Geophys. Res.*, *96*, 869–891, 1991.

Hou, Y.-T., K. A. Campana, and S.-K. Yang, Shortwave radiation calculation in the NCEP's global model, paper presented at RRS '96: Current Problems in Atmospheric Radiation, Int. Radiat. Comm., Fairbanks, Alaska, Aug. 19–24, 1996.

Inamdar, A. K., and V. Ramanathan, Physics of greenhouse and convection in warm oceans, *J. Clim.*, *7*, 715–731, 1994.

Kanamitsu, M., J. C. Alpert, K. A. Campana, P. M. Caplan, D. G. Deaven, M. Iredell, B. Katz, H.-L. Pan, and G. H. White, Recent changes implemented into the global forecast system at NMC, *Weather Forecasting*, *124*, 1145–1160, 1991.

Kiehl, J. T., On the observed near cancellation between longwave and shortwave cloud forcing in tropical regions, *J. Clim.*, *7*, 559–565, 1994.

Kiehl, J. T., and B. P. Briegleb, Comparison of the observed and calculated clear sky greenhouse effect: Implications for climate studies, *J. Geophys. Res.*, *97*, 10,037–10,049, 1992.

Lacis, A. A., and J. E. Hansen, A parameterization for the absorption of solar radiation in the Earth's atmosphere, *J. Atmos. Sci.*, *31*, 118–133, 1974.

Le Dimet, F. X., H. E. Ngodock, and B. Luong, Sensitivity analysis in variational data assimilation, *J. Meteorol. Soc. Jpn.*, *75*, 135–145, 1997.

Li, Y., I. M. Navon, P. Courtier, and P. Gauthier, Variational data assimilation with a semi-implicit global shallow water equation model and its adjoint, *Mon. Weather Rev.*, *121*, 1759–1769, 1993.

Manabe, S., and R. F. Strickler, Thermal equilibrium of an atmosphere with a convective adjustment, *J. Atmos. Sci.*, *21*, 361–385, 1964.

Navon, I. M., X. Zou, J. Derber, and J. Sela, Variational data assimilation with an adiabatic version of NMC spectral model, *Mon. Weather Rev.*, *120*, 1433–1446, 1992.

Palmén, E., and C. W. Newton, *Atmospheric Circulation Systems*, Academic, San Diego, Calif., 1967.

Rabier, F., P. Courtier, and O. Talagrand, An application of adjoint models to sensitivity, *Contrib. Atmos. Phys.*, *65*, 177–192, 1992.

Rabier, F., E. Klinker, P. Courtier, and A. Hollingworth, Sensitivity of forecast errors to initial conditions, *Q. J. R. Meteorol Soc.*, *122*, 121–150, 1996.

Ramanathan, V., R. D. Cess, E. F. Harrison, P. Minnis, B. R. Barkstrom, E. Ahmad, and D. Hartmann, Cloud-radiative forcing and climate: Results from the Earth Radiation Budget Experiment, *Science*, *243*, 57–63, 1989.

Raval, A., and V. Ramanathan, Observational determination of the greenhouse effect, *Nature*, *342*, 758–761, 1989.

Schwarzkopf, M. D., and S. B. Fels, Improvements to the algorithm for computing CO_2 transmissivities and cooling rates, *J. Geophys. Res.*, *90*, 10,541–10,550, 1985.

Schwarzkopf, M. D., and S. B. Fels, The simplified exchange method revisited: An accurate, rapid method for computation of infrared cooling rate and fluxes, *J. Geophys. Res.*, *96*, 9075–9096, 1991.

Sinha, A., and K. P. Shine, Simulated sensitivity of the Earth's radiation budget to changes in cloud properties, *Q. J. R. Meteorol. Soc.*, *121*, 797–819, 1995.

Slingo, A., Sensitivity of the Earth's radiation budget to changes in low clouds, *Nature*, *343*, 49–51, 1990.

Slingo, J. M., The development and verification of a cloud prediction scheme for the ECMWF model, *Q. J. R. Meteorol. Soc.*, *113*, 899–928, 1987.

Stephens, G. L., The parameterization of radiation for numerical weather prediction and climate models, *Mon. Weather Rev*, *112*, 827–846, 1984.

Stephens, G. L., and T. J. Greenwald, The Earth's radiation budget and its relation to atmospheric hydrology, 1, Observations of the clear sky greenhouse effect, *J. Geophys. Res.*, *96*, 15,311–15,324, 1991.

Stokes, G. M., and S. E. Schwartz, The Atmospheric Radiation Measurement (ARM) Program: Programmatic background and design of the cloud and radiation test bed, *Bull. Am. Meteorol. Soc.*, *75*, 1201–1221, 1994.

Talagrand, O., and P. Courtier, Variational assimilation of meteorological observations with the adjoint vorticity equation, I, Theory, *Q. J. R. Meteorol. Soc.*, *113*, 1131–1328, 1987.

Yamanouchi, T., and T. P. Charlock, Comparison of radiation budget at the TOA and surface in the Antarctic from ERBE and ground surface measurements, *J. Clim.*, *8*, 3109–3120, 1995.

Yang, S.-K., A. J. Miller, Y.-T. Hou, and C. F. Ropelewski, Components of the Earth radiation budget in NCEP/NCAR reanalysis, in *Proceedings of the 20th Annual Climate Diagnostic Workshop*, pp. 172–175, Am. Meteorol. Soc., Boston, Mass., 1995.

Zhang, M. H., R. D. Cess, T. Y. Kwon, and M. H. Chen, Approach of comparison for clear-sky radiative fluxes from general circulation models with Earth Radiation Budget Experiment data, *J. Geophys. Res.*, *99*, 5515–5523, 1994a.

Zhang, M. H., J. J. Hank, J. T. Kiehl, and R. D. Cess, Diagnostic study of climate feedback processes in atmospheric general circulation models, *J. Geophys. Res.*, *99*, 5525–5537, 1994b.

Zhang, Y.-C., W. B. Rossow, and A. A. Lacis, Calculation of surface and top of atmosphere radiative fluxes from physical quantities based on ISCCP data sets, 1, Method and sensitivity to input data uncertainties, *J. Geophys. Res.*, *100*, 1149–1165, 1995.

Zou, X., Tangent linear and adjoint of "on-off" processes and their feasibility for use in 4-dimensional variational assimilation, *Tellus*, *Ser. A*, *49*, 3–31, 1997.

Zou, X., A. Barcilon, I. M. Navon, J. Whittaker, and D. G. Cacuci, An adjoint sensitivity study of blocking in a two-layer isentropic model, *Mon. Weather Rev.*, *121*, 2833–2857, 1993.

Z. Li, Supercomputer Computations Research Institute, Florida State University, Tallahassee, FL 32306-4052.

I. M. Navon, Department of Mathematics, Florida State University, Tallahassee, FL 32306-4052. (e-mail: navon@scri.fsu.edu)

(Received April 11, 1997; revised December 4, 1997;
accepted December 11, 1997.)